



Cite this: *Phys. Chem. Chem. Phys.*,  
2015, 17, 25014

# Chemical-shift tensors of heavy nuclei in network solids: a DFT/ZORA investigation of $^{207}\text{Pb}$ chemical-shift tensors using the bond-valence method†

Fahri Alkan and C. Dybowski\*

Cluster models are used in calculation of  $^{207}\text{Pb}$  NMR magnetic-shielding parameters of  $\alpha\text{-PbO}$ ,  $\beta\text{-PbO}$ ,  $\text{Pb}_3\text{O}_4$ ,  $\text{Pb}_2\text{SnO}_4$ ,  $\text{PbF}_2$ ,  $\text{PbCl}_2$ ,  $\text{PbBr}_2$ ,  $\text{PbClOH}$ ,  $\text{PbBrOH}$ ,  $\text{PbIOH}$ ,  $\text{PbSiO}_3$ , and  $\text{Pb}_3(\text{PO}_4)_2$ . We examine the effects of cluster size, method of termination of the cluster, charge on the cluster, introduction of exact exchange, and relativistic effects on calculation of magnetic-shielding tensors with density functional theory. Proper termination of the cluster for a network solid, including approximations such as compensation of charge by the bond-valence (BV) method, is essential to provide results that agree with experiment. The inclusion of relativistic effects at the spin-orbit level for such heavy nuclei is an essential factor in achieving agreement with experiment.

Received 9th June 2015,  
Accepted 31st August 2015

DOI: 10.1039/c5cp03348a

www.rsc.org/pccp

## 1. Introduction

Lead has a rich and diverse co-ordination chemistry, ranging from organometallic compounds<sup>1</sup> to inorganic salts.<sup>2</sup> Solid lead materials often show a variety of structural motifs, *e.g.* the structural features of the various oxides of lead. The large NMR chemical-shift range ( $\sim 10\,000$  ppm) of  $^{207}\text{Pb}$ ,<sup>3,4</sup> and the strong dependence of the NMR chemical shift on co-ordination geometry and electronic structure, makes the study of the  $^{207}\text{Pb}$  nucleus in solid materials an attractive means to analyze them, and reports have appeared in which the experimental shifts are empirically correlated with structure.<sup>5–15</sup> Aside from the isotropic shift, the principal components of the chemical-shift tensor in the solid are sensitive to the local electronic structure.<sup>16</sup> The full chemical-shift tensor provides more details on structural motifs in a solid than a measure of the isotropic chemical shift alone.

The magnetic shielding, as specified by the chemical shift, is a quantum mechanical property of the electronic system, and a characterization of experimental solid-state NMR (SSNMR) results requires calculation of the magnetic shielding for models of the solid state. It is known, from calculations in the literature, that relativistic quantum chemistry methods including spin-orbit (SO) corrections are necessary to produce meaningful theoretical predictions of  $^{207}\text{Pb}$  magnetic-shielding parameters.<sup>17</sup> For a solid, one must also include intermolecular

effects in calculating magnetic shielding, which requires a model of the extended local structure of the system.<sup>18,19</sup> For light nuclei such as  $^{13}\text{C}$  or  $^{29}\text{Si}$ , the gauge included periodic augmented wave (GIPAW) method<sup>20–22</sup> has been shown to produce very good agreement with experiment.<sup>23</sup> However, for systems containing heavy nuclei such as  $^{119}\text{Sn}$ ,  $^{207}\text{Pb}$ , and  $^{199}\text{Hg}$ , the GIPAW method is not as useful due to the lack of inclusion of relativistic spin-orbit effects in the current implementations of the GIPAW algorithm, and the basis sets used have not been optimized for these heavy nuclei.

With the cluster model, one may calculate the magnetic-shielding tensor at various levels of approximation, up to and including spin-orbit effects.<sup>19</sup> Comparison allows one to determine which effects are most important. Several recipes have been proposed to employ clusters in magnetic-shielding calculations.<sup>13–15,24–38</sup> By calculation with clusters of different sizes, the components of the magnetic-shielding tensor tend towards a limit as the size of the cluster is increased. Because the magnetic-shielding tensor depends most strongly on the electronic structure near the nucleus,<sup>39–42</sup> agreement with experiment is obtained with calculations on moderate-size clusters, as discussed below. A combination of a sufficiently large cluster and proper treatment of spin-orbit effects yields good agreement between theory and experiment.<sup>19</sup>

The main disadvantage of the use of cluster models occurs when one attempts to extend these methods to ionic or covalent network solids. In that case, termination of the periodic structure yields dangling bonds and uncompensated positive or negative charge in the model cluster. Quantum chemical modelling of such systems usually yields either non-convergence during the self-consistent-field (SCF) cycle or a difficult convergence,

Department of Chemistry and Biochemistry, University of Delaware, Newark,  
DE 19716-2522, USA. E-mail: dybowski@udel.edu

† Electronic supplementary information (ESI) available. See DOI: 10.1039/c5cp03348a



which signals that the model has a non-physically small HOMO–LUMO gap. The resulting NMR parameters cannot be trusted, and one must seek alternative ways to model the structure.

The high charge or dangling bonds on a model cluster results in incorrect placement of electron density, a situation that would not be found in the extended solid. One solution to this practical problem is to add hydrogens to outer atoms of the cluster (maintaining proper symmetry) to stabilize the cluster. This method has been employed to obtain converged solutions with meaningful NMR parameters in solids for a variety of systems.<sup>24,25,43</sup> Another method to account for this effect is to terminate the cluster with pseudo-atoms generated by changing the nuclear charges ( $Z_{\text{nuc}}$ ) of the cluster's outer atoms that have missing co-ordination. The aim of this procedure is to stabilize the system by reducing the non-compensated charge on the edges of the cluster. Different versions of this methodology have been applied to systems to study energetics of surface reactions computationally.<sup>44–47</sup> To our knowledge, there is no computational study of NMR parameters that has employed this method.

In this contribution, we report calculations of the  $^{207}\text{Pb}$  magnetic-shielding tensor by using clusters extracted from X-ray or neutron diffraction geometries of the corresponding solid. We investigate effects of terminating the cluster, of cluster size, of charge, and of symmetry on calculated magnetic-shielding tensors. We discuss the importance of various relativistic effects on the  $^{207}\text{Pb}$  magnetic-shielding tensor at different levels of relativistic correction. We briefly discuss effects of various methodological differences on the accuracy of calculated  $^{207}\text{Pb}$  magnetic-shielding tensors.

## 2. Computational methods

All computations were performed using the Amsterdam Density Functional (ADF v2014)<sup>48–50</sup> program package. NMR parameters were computed with the NMR module by employing the GIAO formalism.<sup>51–55</sup> Calculations were carried out at the BP86 level.<sup>56,57</sup> For the NMR nuclei and for the first co-ordination shell, the TZ2P basis set was employed at the all-electron level. For the remainder of the cluster, the DZ basis set and the frozen core approximation (FCA)<sup>52,55</sup> were employed to reduce the computational time. Details of the FCA for each individual nucleus, cluster structural information, and results of calculations are given in the ESI.† To include relativistic effects, the zeroth order regular approximation (ZORA)<sup>58–61</sup> was employed at the spin–orbit level, unless otherwise indicated.

### Cluster definition

X-ray or neutron diffraction parameters were used to generate input geometries for the molecular clusters.<sup>62–71</sup> For each solid, the space group and the corresponding Inorganic Crystal Structure Database<sup>6</sup> reference code are given in Table 1. The clusters were created by defining a central NMR-active atom, and successively adding atoms to form clusters with one, three, or five layers of surrounding atoms. Terminal atoms of a cluster

Table 1 Reference codes and crystallographic data for lead-containing solids

Crystal system	Reference code <sup>a</sup>	Space group	Unique Pb(II) sites by symmetry
$\alpha$ -PbO	15466	<i>P4/nmm</i>	1
$\beta$ -PbO	40180	<i>Pbcm</i>	1
Pb <sub>3</sub> O <sub>4</sub>	4106	<i>P4<sub>2</sub>/mbc</i>	1 <sup>b</sup>
Pb <sub>2</sub> SnO <sub>4</sub>	31482	<i>Pbam</i>	2
PbF <sub>2</sub>	154994	<i>Pnma</i>	1
PbCl <sub>2</sub>	27736	<i>Pnma</i>	1
PbBr <sub>2</sub>	202134	<i>Pnma</i>	1
PbClOH	404572	<i>Pnma</i>	1
PbBrOH	404573	<i>Pnma</i>	1
PbIOH	Lutz <i>et al.</i> <sup>69</sup>	<i>Pnma</i>	1
PbSiO <sub>3</sub>	26812	<i>P2/n</i>	3
Pb <sub>3</sub> (PO <sub>4</sub> ) <sub>2</sub>	14247	<i>C2/c</i>	2

<sup>a</sup> Codes from the Inorganic Crystal Structure Database, or structures are from the literature where no code is given. <sup>b</sup> There is also a unique Pb(IV) site for this system.

were treated either by coordinating additional hydrogens to the cluster or by changing the nuclear charge of terminal atoms to ensure SCF convergence. For the hydrogen-addition (HA) method, the hydrogen atoms were coordinated to outer oxygen atoms such that the O–H bond length was 0.96 Å and the Pb–O–H angle was 180°.

For clusters where  $Z_{\text{nuc}}$  was modified for the outer atoms with missing co-ordination, two different methodologies were employed. In the first method, the nuclear charges of the terminal atoms in the cluster were increased by +1. This method we call valence modification of the terminal atoms (VMTA). In this scheme, the total charge on the cluster is the same as in the HA method.

In the second method,  $Z_{\text{nuc}}$  of a terminal atom is modified according to the sum of the bond strengths of that atom. The bond strength ( $S$ ) for a terminal atom is calculated using an equation from the bond-valence model:<sup>72–75</sup>

$$S = \sum_i \exp\left(\frac{R_{i0} - R_i}{b_i}\right) \quad (1)$$

In eqn (1),  $R_i$  is the bond length between two atoms in a pair containing the terminal atom.  $R_{i0}$  and  $b_i$  are fitted bond valence parameters tabulated in a recent review of the bond-valence model.<sup>75</sup> For this study, the parameter  $R_{i0}$  is slightly modified from the reported values,<sup>75</sup> so that the total bond strength of an atom with a complete co-ordination sphere corresponds to the oxidation state of that atom. For the terminal atoms, the bond strength,  $S$ , is calculated using eqn (1) and the modified  $Z_{\text{nuc}}$  of the terminal atom ( $Z_{\text{mod}}$ ) is calculated from:

$$Z_{\text{mod}} = Z_{\text{nuc}} + \Delta S \quad (2)$$

$$\Delta S = V_a - S \quad (3)$$

where  $\Delta S$  is the difference between the valence of the terminal atom,  $V_a$ , and the calculated bond strength of the terminal atom in the cluster. In other words,  $\Delta S$  corresponds to the missing co-ordination bond strength of the terminal atom.



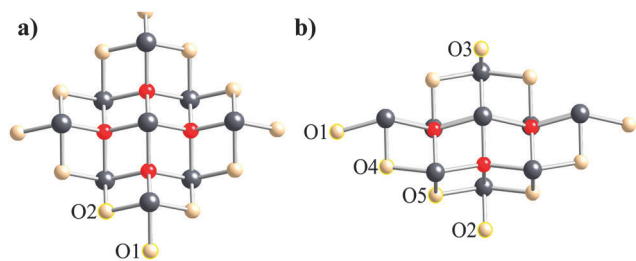


Fig. 1 Different terminal oxygen sites according to bond valence model in (a)  $\alpha$ -PbO and (b)  $\beta$ -PbO.

We refer to this method as the bond-valence approach, or VMTA/BV.

As an example of the VMTA/BV method, terminal oxygen atoms with different coordination spheres are illustrated in Fig. 1a and b for the third co-ordination shell clusters of  $\alpha$ -PbO and  $\beta$ -PbO, respectively. For  $\alpha$ -PbO, there is only one unique Pb–O bond length in the crystal structure. Therefore, the bond strength and  $Z_{\text{mod}}$  of the terminal oxygen atoms only depend on the number of lead atoms coordinated to the terminal oxygen atom. In Fig. 1a, there are two distinct terminal oxygen sites. O1 is coordinated to a single lead site, whereas O2 is coordinated to two lead sites with the same bond length. Calculated bond strengths are 0.50 and 1.00 valence units (vu)<sup>75</sup> for O1 and O2 respectively. Because the bond strength of oxygen having complete coordination (*i.e.*, surrounded by four lead atoms) is 2.00 vu,  $Z_{\text{mod}}$  for each of the two types of terminal oxygen atoms in these clusters is calculated to be 9.50 and 9.00 vu for O1 and O2, respectively. For  $\beta$ -PbO, calculation of bond strengths is not as simple, due to lower symmetry and multiple Pb–O bond lengths in the structure. As a result, there is more variation in the number of distinct terminal oxygen sites. The calculated bond strengths are 0.37, 0.61, 0.64, 0.99, and 1.01 vu for O1 to O5, respectively.

The effect of VMTA/BV on the energy levels of a cluster is illustrated in Fig. 2 for the third co-ordination shell geometry of  $\alpha$ -PbO. For a cluster without any treatment of the terminal

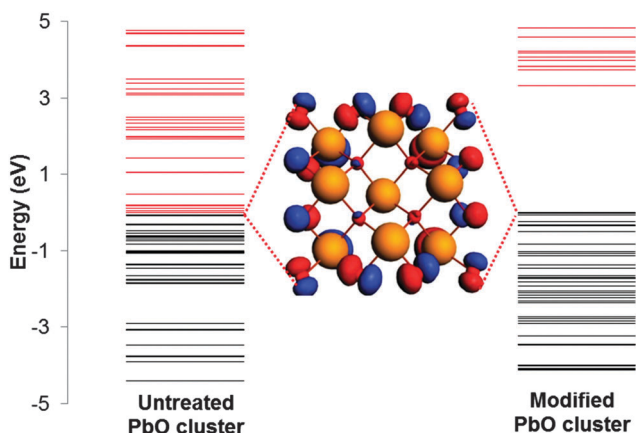


Fig. 2 Energy levels for the 3rd co-ordination cluster of  $\alpha$ -PbO. The occupied levels are shown in black whereas unoccupied levels are shown in red. These qualitative calculations carried out with BP86 functionals and the ZORA spin-orbit Hamiltonian.

atoms, there is no clear difference in energy between the HOMO and LUMO levels. As a result, convergence under SCF is difficult or impossible as the algorithm becomes oscillatory. Upon closer inspection, it is seen that frontier MOs are mostly dominated by the p orbitals of the terminal oxygen atoms. When  $Z_{\text{nuc}}$  for the atoms is adjusted as described, these levels are stabilized, due to an additional component of the nuclear potential that creates the energy difference between the HOMO and LUMO levels. As a result, SCF convergence is achieved easily for clusters modified with VMTA/BV.

### Magnetic shielding

The magnetic shielding of a nucleus is a tensor property,  $\sigma$ , which can be represented as a  $3 \times 3$  matrix in a Cartesian co-ordinate system.

$$\sigma = \begin{bmatrix} \sigma_{xx} & \sigma_{xy} & \sigma_{xz} \\ \sigma_{yx} & \sigma_{yy} & \sigma_{yz} \\ \sigma_{zx} & \sigma_{zy} & \sigma_{zz} \end{bmatrix} \quad (4)$$

In its principal-axis system, the diagonal elements are known as the principal components of the tensor. These principal components are assigned as:  $\sigma_{11} \leq \sigma_{22} \leq \sigma_{33}$ , which is known as the frequency-ordered convention.<sup>76</sup>

In the NMR experiment, the chemical shift, the shielding relative to the (usually isotropic) resonance position of some reference material, is reported. The principal components of the magnetic-shielding tensor and the principal chemical-shift components are related by eqn (5).

$$\delta_{ii} = \frac{\sigma_{\text{ref}} - \sigma_{ii}}{1 - \sigma_{\text{ref}}} \quad (5)$$

In principle, one defines the chemical-shift tensor experimentally with the three principal components,  $\delta_{11}$ ,  $\delta_{22}$ , and  $\delta_{33}$ . There are several other descriptions in use. In one convention, the tensor is expressed in terms of its irreducible spherical-tensor components.<sup>77</sup> Another convenient description for spectra of powders is given by the Maryland convention, a set of three NMR parameters describing the shape of the spectrum of a random powder sample, the isotropic chemical shift ( $\delta_{\text{iso}}$ ), the span ( $\Omega$ ), and the skew ( $\kappa$ ).<sup>76</sup> These three parameters are related to the principal components of the chemical-shift tensor by the following relations:

$$\delta_{\text{iso}} = \frac{1}{3}(\delta_{11} + \delta_{22} + \delta_{33}) \quad (6a)$$

$$\Omega = \delta_{11} - \delta_{33} \quad (6b)$$

$$\kappa = \frac{3(\delta_{22} - \delta_{\text{iso}})}{\Omega} \quad (6c)$$

## 3. Calculations for $\alpha$ -PbO and $\beta$ -PbO

### 3.1. Effects of termination method and cluster size on calculated NMR parameters

We investigate modelling of PbO clusters of different sizes, as well as the effects of cluster size on predicted principal components of the shielding tensor, by the HA, VMTA and VMTA/BV



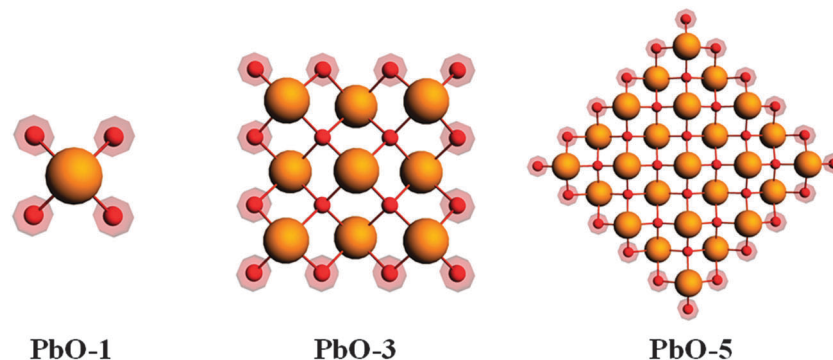


Fig. 3 1st, 3rd and 5th co-ordination shell geometries of  $\alpha$ -PbO. The terminal oxygen atoms are shown in red circles. The corresponding  $\beta$ -PbO clusters have the same bonding network with differences in bond lengths and angles.

methods. Clusters up to the first, third, and fifth atomic co-ordination shells around the NMR nucleus are shown in Fig. 3. Only the odd-numbered co-ordination shells are considered, because clusters terminated with lead atoms are inherently difficult to handle computationally. The calculated NMR parameters for clusters of the two different forms of PbO ( $\alpha$ -PbO and  $\beta$ -PbO) using the HA, VMTA, and VMTA/BV methods are given in Table 2. The method used in each case is given by its abbreviation and the prefix gives the maximum co-ordination shell in the cluster. In Table 2, the reduced chemical shifts are defined by the following relation:

$$\Delta\delta_{ii} = \delta_{ii} - \delta_{\text{iso}} = \sigma_{\text{iso}} - \sigma_{ii} \quad (7)$$

For  $\alpha$ -PbO and  $\beta$ -PbO, the predicted values of the principal shielding components for a cluster model terminated at the first co-ordination sphere strongly depend on the termination method, with values that can be different from one another by more than 2000 ppm. On the other hand, for clusters of  $\alpha$ -PbO and  $\beta$ -PbO including atoms up to the third co-ordination shell, the predicted values of the principal shielding components are significantly less dependent on the termination method. For example, the largest difference between values found with different methods (in this case, VMTA and HA) is only 343 ppm, which is the deviation for  $\sigma_{11}$  ( $= \sigma_{22}$ ) of  $\alpha$ -PbO. There are only small differences in the principal components calculated by the VMTA or the VMTA/BV method, showing that these two methods are similar. The maximum difference for calculated

Table 2 Principal components of the  $^{207}\text{Pb}$  magnetic-shielding tensor and reduced chemical shifts for various cluster models of  $\alpha$ -PbO and  $\beta$ -PbO

	$\sigma_{11}$ (ppm)	$\sigma_{22}$ (ppm)	$\sigma_{33}$ (ppm)	$\sigma_{\text{iso}}$ (ppm)	$\Delta\delta_{11}$ (ppm)	$\Delta\delta_{22}$ (ppm)	$\Delta\delta_{33}$ (ppm)	$\Omega$ (ppm)	Residual <sup>a</sup>
<b><math>\alpha</math>-PbO</b>									
Experiment <sup>8</sup>					1100	1100	-2200	3300	—
1-HA	9400	9400	10 645	9815	415	415	-830	1244	969
1-VMTA	7385	7385	9681	8151	765	765	-1531	2296	473
1-VMTA/BV	9451	9451	11 269	10 057	606	606	-1212	1818	699
3-HA	6204	6204	8918	7109	905	905	-1809	2714	276
3-VMTA	5861	5861	8870	6864	1003	1003	-2006	3010	137
3-VMTA/BV	5887	5889	8827	6868	981	979	-1960	2940	170
5-HA	5935	5935	8922	6931	995	995	-1991	2986	148
5-VMTA	5936	5936	8906	6926	990	990	-1980	2970	156
5-VMTA/BV	5914	5915	8900	6910	996	994	-1990	2986	148
<b><math>\beta</math>-PbO</b>									
Experiment <sup>8</sup>					1293	1233	-2527	3820	—
1-HA	9125	9533	10 871	9843	718	310	-1028	1746	1069
1-VMTA	7109	7525	9537	8057	948	532	-1480	2428	754
1-VMTA/BV	8630	9283	11 516	9810	1180	527	-1706	2886	629
3-HA	5956	6406	9270	7211	1255	805	-2059	3314	367
3-VMTA	5747	6228	9273	7083	1335	855	-2190	3525	294
3-VMTA/BV	5655	6197	9352	7068	1413	871	158	3697	261
5-HA	6136	6150	9630	7305	1169	1155	-2324	3493	144
5-VMTA	6098	6172	9593	7288	1190	1115	-2305	3495	157
5-VMTA/BV	6100	6150	9581	7277	1177	1127	-2304	3481	158

$$^a \text{Residual} = \sqrt{\frac{1}{3} \sum_{i=1}^3 (\Delta\delta_{ii}^{\text{calc}} - \Delta\delta_{ii}^{\text{exp}})^2}$$



components by these two methods is no greater than 100 ppm.

For clusters that include the fifth co-ordination shell of  $\alpha$ -PbO or  $\beta$ -PbO, the principal components calculated using the three termination methods agree to within 50 ppm. This agreement reflects the fact that the various termination methods have little effect on the shielding values calculated for fifth-coordination-sphere clusters chosen to represent these network solids.

A comparison of the calculated values to experimental results<sup>8</sup> is illustrated with the residuals of the components of the reduced chemical-shift tensor [Table 2]. These residuals are generally smaller for larger clusters. For clusters containing only the first co-ordination shell, the residuals range from 473 ppm to 1069 ppm. For clusters containing up to the third co-ordination shell, the residuals range from 137 ppm to 367 ppm. For clusters containing up to the fifth co-ordination shell, the residuals range only from 144 to 158 ppm. The larger the clusters, regardless of termination method, the closer the calculated components are to the experimental components.

### 3.2. Symmetry requirements for calculated principal components

The local symmetry of the electronic environment surrounding the NMR-active nucleus affects the values of the principal components of the magnetic-shielding tensor.<sup>78</sup> We have deliberately perturbed the symmetry of cluster models of  $\alpha$ -PbO to determine the extent of this effect. In Fig. 4 is shown an example, in which a fifth-coordination-shell cluster model is perturbed by adding up to the seventh coordination shell along the +x axis. For the calculated magnetic-shielding parameters in Table 3, we have used models extended by two coordination shells in the +x direction for the first-, third-,

Table 3 Principal components of the <sup>207</sup>Pb magnetic-shielding tensors of symmetric and perturbed clusters of  $\alpha$ -PbO

$\alpha$ -PbO	$\sigma_{11}$ (ppm)	$\sigma_{22}$ (ppm)	$\sigma_{33}$ (ppm)	$\sigma_{iso}$ (ppm)	$\Omega$ (ppm)	$\kappa$
1sym <sup>a</sup>	9451	9451	11 269	10 057	1818	1.00
1pert <sup>b</sup>	8183	8578	10 964	9241	2781	0.72
Difference	1268	873	305	816	−963	0.28
3sym <sup>a</sup>	5887	5889	8827	6868	2940	1.00
3pert <sup>b</sup>	5734	5875	8737	6782	3004	0.91
Difference	153	14	90	86	−64	0.09
5sym <sup>a</sup>	5914	5915	8900	6910	2986	1.00
5pert <sup>b</sup>	5906	5909	8888	6901	2982	1.00
Difference	8	6	2	9	4	0.00

<sup>a</sup> Symmetric cluster. <sup>b</sup> Perturbed cluster.

and fifth-coordination-shell cluster models to lower the symmetry at the site of the NMR-active nucleus.

From the X-ray crystal structure, Pb sites in  $\alpha$ -PbO have  $C_{4v}$  site symmetry.<sup>62</sup> By symmetry constraints, the skew ( $\kappa$ ) is either  $-1.00$  ( $\sigma_{11} < \sigma_{22} = \sigma_{33}$ ) or  $+1.00$  ( $\sigma_{11} = \sigma_{22} < \sigma_{33}$ ). Experimentally,  $\alpha$ -PbO has a skew of  $+1.00$ .<sup>6,8,79</sup> Calculated NMR parameters for the symmetric and perturbed clusters are presented in Table 3.

For a cluster that contains the first co-ordination shell, the differences between principal components of symmetric and perturbed clusters are 1268, 873 and 305 ppm for  $\sigma_{11}$ ,  $\sigma_{22}$  and  $\sigma_{33}$ , respectively, with a predicted  $\kappa$  of 0.72 for the perturbed structure. For a cluster that includes the third co-ordination shell,  $\kappa$  is 0.91, only 0.09 from the ideal value. For this cluster model, the differences range only between 153 and 14 ppm for the principal components. For a model containing co-ordination shells through the fifth, the differences between the calculated principal components of the perturbed and symmetric models are very small. The calculated  $\kappa$  for both clusters are  $+1.00$ , within 1%. These results, along with the results in Table 2, indicate that the principal values of the magnetic-shielding tensor converge to a limit for a cluster that contains up to the fifth co-ordination shell of <sup>207</sup>Pb. Deviations from symmetry occurring at the edges of a cluster of sufficient size seem to have minimal effects on the derived magnetic-shielding tensor and its symmetry at this level of precision. For other nuclei, the limit may depend on the nucleus and the local structure.

### 3.3. Effects of the charge on the terminal atoms

For  $\alpha$ -PbO, the VMTA/BV method predicts 9.50 and 9.00 for  $Z_{mod}$  of the two types of terminal oxygen atoms (O1 and O2 in Fig. 1). We investigate how the value of  $Z_{mod}$  in the range of 9.30 to 9.70 and 8.80 to 9.20 for these two sites, respectively, affects the predicted NMR magnetic-shielding parameters. For these models, the total charge on a cluster depends on the size of the cluster as well as  $Z_{mod}$  of the two terminal oxygen sites, as indicated in Table 4. As seen in Fig. 5,  $\sigma_{iso}$  and  $\Omega$  are linearly correlated with the deviation,  $\Delta Z_{mod}$ , of  $Z_{mod}$  from the optimal values (9.50 and 9.00). For the cluster containing up to only the first co-ordination sphere, the variation of the isotropic shielding and the span with  $Z_{mod}$  is large. In changing  $Z_{mod}$  by 0.4, the isotropic magnetic shielding varies by over 2000 ppm and

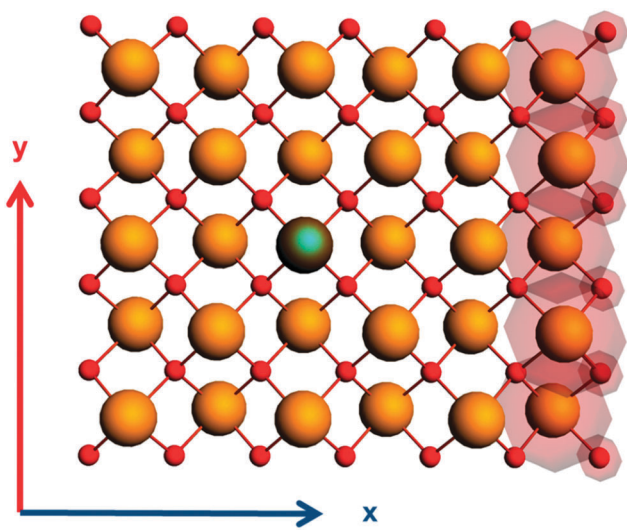


Fig. 4 Distorted 5th co-ordination shell cluster of  $\alpha$ -PbO. The added co-ordination in x-direction is shown in red circles whereas the central <sup>207</sup>Pb nuclei is highlighted.



**Table 4** Dependence of the predicted magnetic-shielding tensor of  $\alpha$ - $^{207}\text{PbO}$  on the total charge on a cluster extending to the fifth co-ordination shell

$Z_{\text{mod}}$ on O1 and O2	Total charge on cluster	Mulliken charge on Pb	Mulliken				
			$\sigma_{11}$ (ppm)	$\sigma_{22}$ (ppm)	$\sigma_{33}$ (ppm)	$\sigma_{\text{iso}}$ (ppm)	$\Omega$ (ppm)
9.30, 8.80	-4.0	1.344	6005	6006	8959	6990	2954
9.40, 8.90	-2.0	1.364	5957	5959	8928	6948	2971
9.50, 9.00	0.0	1.381	5914	5915	8900	6910	2986
9.60, 9.10	2.0	1.395	5874	5876	8873	6874	2999
9.70, 9.20	4.0	1.408	5839	5841	8848	6843	3009

the span varies by over 1000 ppm. On the other hand, for the largest cluster (through the fifth co-ordination sphere), the isotropic shielding differs by 157 ppm and the span varies by 55 ppm, at most, showing the lack of sensitivity to  $Z_{\text{mod}}$  in large clusters.

The modification of the charge,  $Z_{\text{mod}}$ , on the terminal oxygen atoms is partially delocalized onto other atoms in the cluster. As an example, from Table 4, there is a small, but strong, positive correlation between the Mulliken charge on the central lead atom and  $Z_{\text{mod}}$  of the terminal oxygen sites in this fifth-co-ordination-shell model. In addition, the magnetic-shielding components are correlated with the Mulliken charge on the central lead atom, showing that magnetic shielding reflects the delocalization of charge. The change in the principal components of magnetic shielding with the Mulliken charge demonstrates that there is a somewhat stronger effect on the two degenerate components ( $\sigma_{11}$  and  $\sigma_{22}$ ) than on the unique component ( $\sigma_{33}$ ). This difference between the unique component and the non-unique components in their dependence on delocalization of charge suggests that more electron density from delocalization ends up in orbitals the principal direction of which is in the 1–2 plane, rather than in orbitals whose orientation is perpendicular to that plane. This change is also reflected in the gradual change of  $\Omega$  with total charge on the cluster. These variations of magnetic-shielding parameters with charge on the cluster are even stronger for smaller clusters, as shown in Fig. 5.

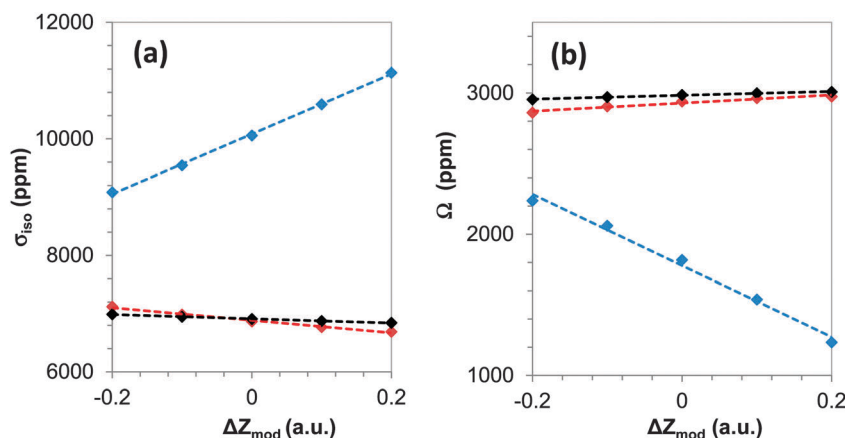


**Fig. 5** The effect of  $Z_{\text{mod}}$  on (a) isotropic shielding and (b) span for models that extend through the first (blue), third (red), and fifth (black) co-ordination shell for  $\alpha$ -PbO.  $\Delta Z_{\text{mod}}$  is the deviation of  $Z_{\text{mod}}$  from the optimal values determined by the VMTA/BV method.

## 4. $^{207}\text{Pb}$ magnetic shielding tensors for various systems

### 4.1. Cluster size

We present a comparison of experimental and calculated principal components of the  $^{207}\text{Pb}$  shielding tensors for a variety of materials (Table 1). The calculations are carried out with two cluster models, the first including only the first co-ordination shell and the second including atoms through the third co-ordination shell.<sup>80</sup> Examples of the clusters are given in Fig. 6. For the terminal atoms in the clusters, VMTA/BV modelling (discussed in Section 2) is employed to reduce charge on the cluster, which also ensures SCF convergence. In this model, the bond strengths are calculated using eqn (1), with parameters,  $R_{i0}$  and  $b_i$ , tabulated in the ESI.†

The relationship between experimental and calculated principal components of the  $^{207}\text{Pb}$  shielding tensors of these various materials is displayed in Fig. 7a for the first-co-ordination-shell model and in Fig. 7b for the third-co-ordination-shell model. Results for the first-co-ordination-shell model show a strong scatter of the data, with  $R^2$  of only 0.608 for a linear correlation. Even for qualitative predictions, NMR parameters obtained using the first-co-ordination-shell model to represent the structure cannot be trusted for these kinds of network solids, as compared to the situation for molecular solids,<sup>19</sup> and we do not report calculations with this model in subsequent analyses.

Use of a model that includes structure through the third co-ordination shell greatly improves the correlation between experimental and calculated principal components, as can be seen in Fig. 7b. For a linear correlation,  $R^2 = 0.983$ . The slope of the best-fit linear correlation line is  $-0.869$ , with an intercept of 8643 ppm. The slope of the correlation line deviates by 13% from the ideal case, which has a slope of  $-1$ .

The predicted absolute magnetic shielding of the reference material, tetramethyllead (TML), from a linear correlation is 9990 ppm for the model that includes only up to the first co-ordination shell. A similar linear correlation of the third-co-ordination-shell model gives a value of 8653 ppm. The absolute



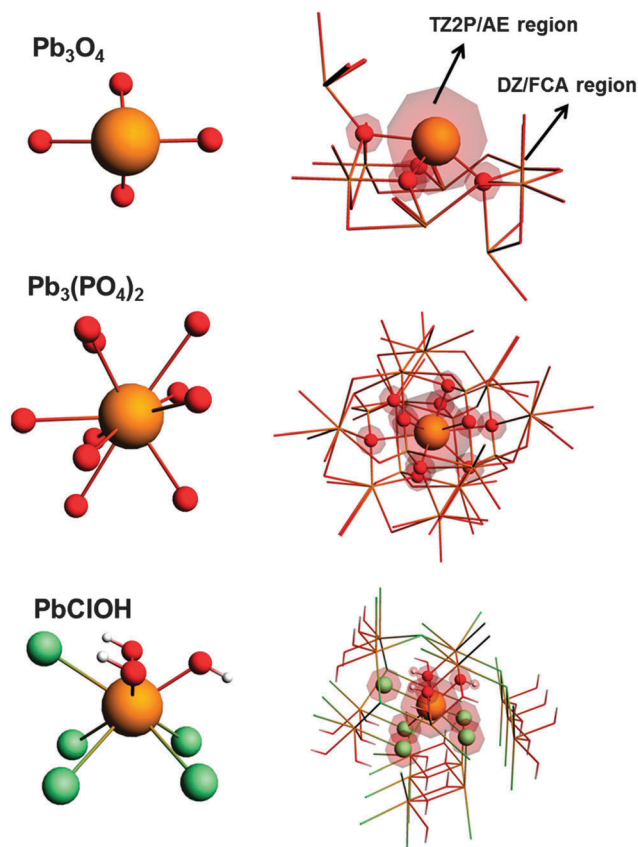


Fig. 6 1st and 3rd co-ordination shell clusters for selective systems investigated in this work. The TZ2P/AE (all-electron) region is shown in the ball-and-stick model, whereas region where FCA/DZ is used is shown by a stick model.

shielding of TML calculated from a model of the molecular solid based on the reported X-ray structure<sup>19</sup> with optimized hydrogen atom positions gives a value of the isotropic shift of

TML of 8136 ppm. There is a significant difference between this estimated shielding of TML and that extracted from the linear correlation of Fig. 7a. On the other hand, the value extracted from Fig. 7b is much closer to the predicted shielding of TML based on its solid-state structure.

#### 4.2. Relativistic effects

In general, for heavy atoms, the contributions to the shielding due to the relativistic nature of the electrons are significant.<sup>19,81–85</sup> For the third-co-ordination-shell model, we compare magnetic-shielding tensors of the suite of materials in Table 1 determined with inclusion of only scalar relativistic corrections to the magnetic-shielding tensors determined above using the full spin-orbit relativistic Hamiltonian. The treatment is at the ZORA/DFT level of theory. Correlation of experimental and theoretical principal components and spans is shown in Fig. 8.

The slope of the correlation line for shielding principal components with experimental chemical-shift components is  $-0.365$  when only scalar relativistic effects are included, whereas the slope of the correlation line for magnetic-shielding principal components when the full relativistic Hamiltonian is used is  $-0.869$ . Neither is the ideal value of  $-1$ , but the inclusion of spin-orbit relativistic terms gives a correlation much closer to the ideal than does the inclusion of only scalar relativistic effects in the ZORA Hamiltonian, showing that spin-orbit terms cannot be neglected in calculations of magnetic shieldings of <sup>207</sup>Pb. We have observed a similar result for the <sup>199</sup>Hg magnetic shielding of solids.<sup>19</sup>

The predicted magnetic shielding of TML from the correlation at the scalar relativistic level is 7060 ppm, whereas a calculation for TML at this scalar relativistic level gives a shielding of 5171 ppm, a difference of 1889 ppm. This difference of 507 ppm indicates that inclusion of the spin-orbit correction is essential to achieve better agreement with the calculated reference shielding from calculation on the reference molecule.

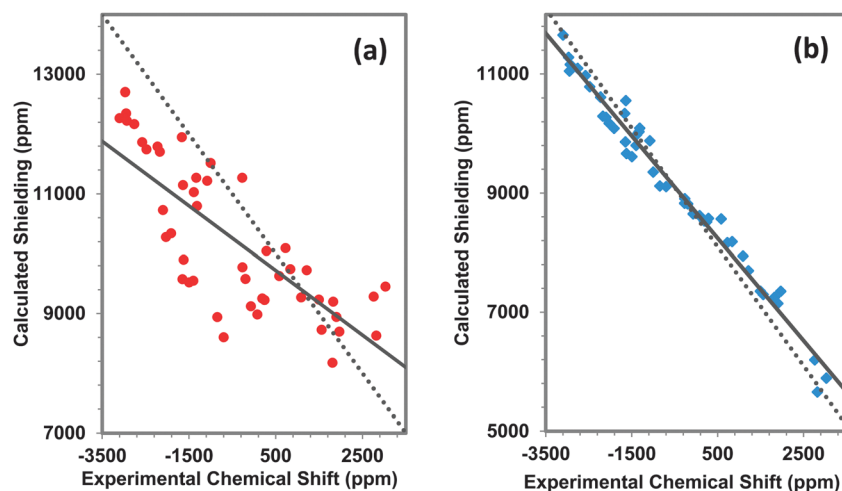
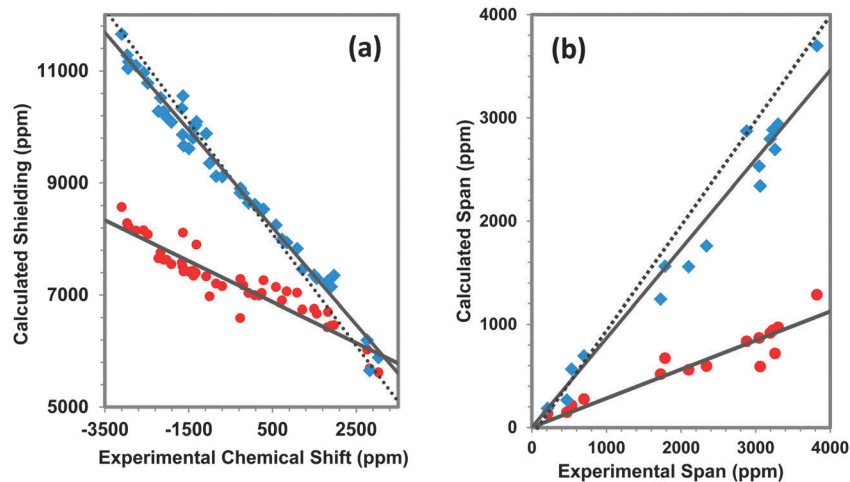


Fig. 7 The correlation between experimental and calculated principal components for (a) the first co-ordination-shell model (●) and (b) the third co-ordination-shell model (◆). The equation of the linear correlation line for the first-co-ordination-shell model is:  $\sigma_{\text{cal}} = -0.541\delta_{\text{exp}} + 9990$  with  $R^2 = 0.608$ . For the third-co-ordination-shell model, the linear correlation is expressed as:  $\sigma_{\text{cal}} = -0.869\delta_{\text{exp}} + 8643$  with  $R^2 = 0.983$ . The dotted line shows ideal behavior (with a slope of  $-1$ ).





**Fig. 8** (a) The correlation between principal components of the magnetic shielding and experimental chemical shift of various lead-containing solids: (●) with inclusion of only scalar relativistic terms; (◆) with inclusion of all relativistic corrections through spin–orbit effects. (b) The correlation of magnetic-shielding span with experimental span of the various lead-containing solids: (●) with inclusion of only scalar relativistic terms; (◆) with inclusion of all relativistic corrections through spin–orbit effects. The calculations were carried out on a third-co-ordination-shell model at the ZORA/DFT level. The equation of the correlation line for the principal components is:  $\sigma_{\text{cal}} = -0.365\delta_{\text{exp}} + 7060$  with  $R^2 = 0.887$  for ZORA/scalar calculations, and  $\sigma_{\text{cal}} = -0.869\delta_{\text{exp}} + 8643$  with  $R^2 = 0.983$  for ZORA/spin–orbit calculations. For the span, the correlation is:  $\Omega_{\text{cal}} = 0.281\Omega_{\text{exp}}$  with  $R^2 = 0.871$  for ZORA/scalar calculations and  $\Omega_{\text{cal}} = 0.866\Omega_{\text{exp}}$  with  $R^2 = 0.962$  for ZORA/spin–orbit calculations. The dotted line shows ideal behavior.

The span of a tensor is independent of the reference. In Fig. 8b, we show the correlation of the predicted and experimental spans for these lead-containing solids. At the ZORA/scalar level of theory, the slope of the best-fit linear correlation of 0.281 deviates significantly from the ideal value of +1. At the ZORA/spin orbit level of theory, the slope of the best-fit linear correlation is 0.866, much closer to the ideal value. This disparity again demonstrates that spin–orbit terms must be included in calculations of magnetic shielding of  $^{207}\text{Pb}$  solids.

One striking feature of Fig. 8b is that the predicted NMR parameters obtained by use of the scalar relativistic terms only systematically underestimate the span of the shielding tensor ( $\sigma_{33} - \sigma_{11}$ ), as compared to values calculated at the spin–orbit level. The spin–orbit calculation also underestimates the span as compared to the experiment, but by a substantially smaller difference. Similar results have been shown for  $^{207}\text{Pb}$ , as well as for  $^{199}\text{Hg}$ .<sup>13,19</sup>

#### 4.3. Accuracy of calculated principal components of the $^{207}\text{Pb}$ shielding tensor

We have shown in the sections above that it is possible to achieve a good correlation between experimental and theoretical principal components of a wide array of lead-containing materials, provided one uses the full spin–orbit-including Hamiltonian at the ZORA level and creates clusters using the VMTA/VB model with inclusion of structure at least to the third co-ordination shell. Even at this level of approximation, the correlation between predicted and experimental results may deviate from the ideal case (in which the slope of the correlation line is exactly  $-1$ ).

**Clusters and the VMTA/BV model.** In Sections 3.1 and 4.1, it is seen that one must include extended solid-state effects by using structural models that account for contributions to the magnetic shielding from atoms in at least the third co-ordination shell about

the nucleus of interest. Inclusion of effects through the fifth co-ordination shell demonstrates that agreement slightly improves by the addition of further atoms. However, as seen in Fig. 9, the slope of the correlation lines approaches the ideal case by about 2%, but the improvement in fit is negligible, suggesting that extending the cluster further is likely to give no substantial improvement in agreement between theory and experiment.

Cluster models, without the use of VMTA/BV theory, have been applied to calculations of  $^{207}\text{Pb}$  principal components in other solid systems.<sup>13,15</sup> In those examples, the ZORA/spin–orbit Hamiltonian was applied at the BP86 level of density functional theory, and no additional treatment was applied to the terminal atoms. For all investigated systems, the span,  $\Omega$ , is consistently underestimated by the model, whether in molecular<sup>13,15</sup> or network solids. This underestimation cannot therefore be attributed to the use of VMTA/BV for termination of the cluster.

**Relativistic effects at the ZORA/spin–orbit Level.** The importance of relativistic effects on shielding of heavy nuclei is well-established.<sup>17,81–90</sup> The present results indicate the necessity of inclusion of spin–orbit effects for calculation of magnetic shielding for these heavy nuclei. It has been shown that the absolute shielding constants for heavy nuclei calculated with ZORA at the spin–orbit level differ considerably from results that are carried out by four-component relativistic methods.<sup>82–85</sup> Autschbach has shown that this difference mainly results from hyperfine integrals involving the core levels.<sup>91</sup> He has also shown that the hyperfine integrals over the valence shells may be evaluated at the ZORA level with accuracy close to that achievable by calculation with the four-component relativistic methods.<sup>91</sup> As a result, the heavy-nucleus chemical shifts determined at the ZORA level of approximation agree well with those calculated with the four-component formalism.<sup>83–85,91</sup> For molecular solids like some Hg-containing materials, the principal components of



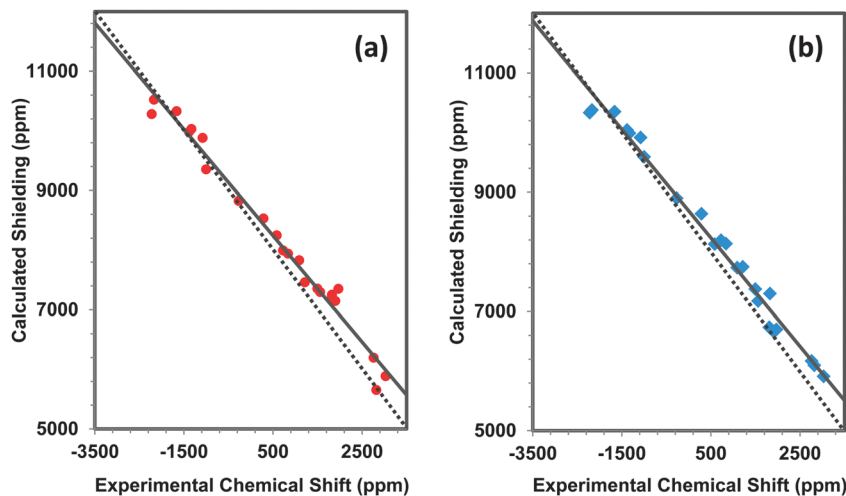


Fig. 9 A comparison of the correlation of the principal components of the experimental chemical-shift tensor and the predicted shielding tensor for  $\alpha$ -PbO,  $\beta$ -PbO,  $\text{Pb}_2\text{SnO}_4$ ,  $\text{Pb}_3\text{O}_4$  and  $\text{PbSiO}_3$  using (a) third- (●) and (b) fifth-co-ordination-shell cluster models. The equation of the correlation line for the third-co-ordination-shell models is:  $\sigma_{\text{cal}} = -0.891\delta_{\text{exp}} + 8689$  with  $R^2 = 0.983$ . For the fifth-co-ordination-shell model, the correlation line is  $\sigma_{\text{cal}} = -0.910\delta_{\text{exp}} + 8690$  with  $R^2 = 0.986$ . The dotted line shows ideal behavior.

chemical-shift tensors have been shown to be predicted with good accuracy using the ZORA Hamiltonian.<sup>19</sup> The present results show that  $^{207}\text{Pb}$  chemical shifts of network solids calculated at the ZORA level of approximation also agree reasonably well with experiment. To our knowledge, there are no reported calculations of  $^{207}\text{Pb}$  chemical shifts with the four-component formalism, but the present results obtained with the ZORA approximation suggest that they would also be in agreement.

**Effect of the density functional by introducing exact exchange.** GGA functionals are the common choice for relativistic magnetic-shielding calculations due to efficient scaling of the methods in both SCF and NMR routines. For light nuclei such as  $^{13}\text{C}$  and  $^{29}\text{Si}$ , introducing exact exchange (*via* hybrid functionals) improves the correlation between experimental and calculated chemical shifts.<sup>92</sup> Recently, hybrid density functionals have been introduced for relativistic calculations of magnetic shielding and spin-spin coupling constants.<sup>81,85,93</sup>

In Table 5, the principal components and spans of  $^{207}\text{Pb}$  magnetic-shielding tensors for five materials are evaluated, with the BP86 and B3LYP<sup>94,95</sup> functionals, on a third-co-ordination-shell cluster. There are two characteristics of the shielding parameters determined by the calculations with B3LYP and with BP86. Firstly, the difference of the B3LYP and BP86 values of  $\sigma_{33}$  for a particular material is always larger than the difference of either  $\sigma_{11}$  or  $\sigma_{22}$ . Secondly, the spans,  $\Omega$ , calculated with B3LYP are always larger than those calculated with BP86. In comparing to experiment,<sup>6,8</sup> the predicted span determined with B3LYP is always closer to the experiment than spans calculated with BP86.

In Fig. 10, the correlation between experimental and calculated principal components of  $^{207}\text{Pb}$  shielding tensors at the BP86 and B3LYP levels of theory are shown. As expected from the comparison of spans,  $\Omega$ , the slope of the correlation line determined with the hybrid functional (B3LYP) is  $-0.985$ , much closer to the ideal value than the correlation line for the same parameters determined at the BP86 level of theory ( $-0.895$ ), demonstrating that the use of hybrid

Table 5 Predicted principal components of  $^{207}\text{Pb}$  magnetic-shielding tensors, determined at either the ZORA/BP86 level of theory or the ZORA/B3LYP level of theory on a cluster extending to the third co-ordination shell

	$\sigma_{11}$ (ppm)	$\sigma_{22}$ (ppm)	$\sigma_{33}$ (ppm)	$\sigma_{\text{iso}}$ (ppm)	$\Omega$ (ppm)
<b>BP86</b>					
$\alpha$ -PbO	5887	5889	8827	6868	2940
$\beta$ -PbO	5655	6197	9352	7068	3697
$\text{PbSiO}_3$ (site 1)	7459	7995	10 331	8595	2872
$\text{PbSiO}_3$ (site 2)	7829	8249	10 522	8867	2693
$\text{PbSiO}_3$ (site 3)	7940	8532	10 281	8918	2341
<b>B3LYP</b>					
$\alpha$ -PbO	5862	5865	8919	6882	3058
$\beta$ -PbO	5572	6119	9587	7092	4015
$\text{PbSiO}_3$ (site 1)	7419	7960	10 551	8643	3133
$\text{PbSiO}_3$ (site 2)	8009	8484	11 030	9174	3021
$\text{PbSiO}_3$ (site 3)	8027	8679	10 710	9139	2683

functionals accounts for contributions to the magnetic shielding more completely than the use of GGA functionals like BP86.

**Experimental uncertainty.** Due to the challenging nature of the spectroscopy of nuclei like  $^{207}\text{Pb}$  having wide powder patterns, there are uncertainties associated with the experimental data. This uncertainty affects the quality of comparisons like those in Fig. 10. In addition, uncertainty about structural parameters derived from X-ray or neutron diffraction measurements contribute to uncertainty in the predicted values. In Table 6 are the results of several reports of experimental chemical-shift parameters of  $\alpha$ -PbO and  $\beta$ -PbO.<sup>6,8,79</sup> The measured principal components may vary by as much as 200 ppm, depending on the report. Averaging these three independent measurements, one obtains average values with uncertainties of up to 200 ppm, as given in Table 6. The uncertainty in principal components ranges from about 50 to 170 ppm. The uncertainties in the span, which is independent of the reference, are 190 ppm and 146 ppm (about 5–6%),



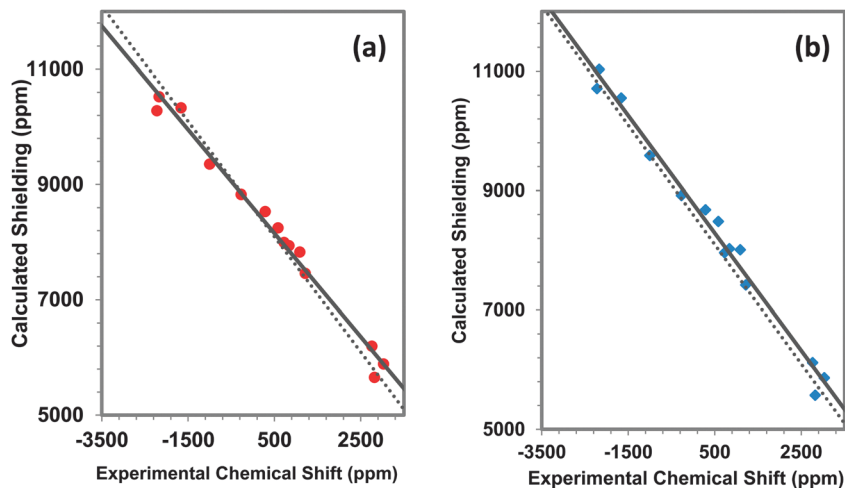


Fig. 10 The comparison of the use of (a) BP86 (●) and (b) B3LYP (◆) to calculate the principal components of sites in  $\alpha$ -PbO,  $\beta$ -PbO and PbSiO<sub>3</sub> for the third-co-ordination-shell model. The equation of the correlation line for the model using BP86 is:  $\sigma_{\text{cal}} = -0.895\delta_{\text{exp}} + 8605$  with  $R^2 = 0.987$ . The equation of the correlation line for the model using B3LYP is:  $\sigma_{\text{cal}} = -0.985\delta_{\text{exp}} + 8781$  with  $R^2 = 0.987$ . The dotted line shows ideal behavior. The values of the slope show how use of B3LYP approaches the ideal behavior.

Table 6 Experimental <sup>207</sup>Pb chemical-shift tensors of the two forms of PbO

	$\delta_{11}$ (ppm)	$\delta_{22}$ (ppm)	$\delta_{33}$ (ppm)	$\delta_{\text{iso}}$ (ppm)	$\Omega$ (ppm)
$\alpha$ -PbO					
Gabuda <i>et al.</i> <sup>8</sup>	3030	3030	-270	1930	3300
Fayon <i>et al.</i> <sup>6</sup>	2977	2977	-137	1939	3114
Zhao <i>et al.</i> <sup>79</sup>	2984	2984	-334	1878	3318
Average	2997 ± 48	2997 ± 48	-247 ± 169	1916 ± 55	3244 ± 190
$\beta$ -PbO					
Gabuda <i>et al.</i> <sup>8</sup>	2820	2760	-1000	1527	3820
Fayon <i>et al.</i> <sup>6</sup>	2945	2573	-972	1515	3917
Zhao <i>et al.</i> <sup>79</sup>	2953	2695	-1040	1536	3993
Average	2906 ± 126	2676 ± 160	-1004 ± 58	1526 ± 18	3910 ± 146

implying that we cannot distinguish the experimental values differing by less than about 100 ppm.

Apart from approximations in the computational formalism that may contribute to the uncertainty in predicted values of the principal components, the uncertainty may also reflect uncertainty in X-ray and neutron diffraction structural parameters used in the definition of the cluster. Dmitrenko *et al.*<sup>14,32</sup> showed that calculated <sup>207</sup>Pb chemical-shift parameters can vary significantly for small changes in bond length and bond angle. They also show that calculated NMR parameters may vary by as much as 200 ppm, depending on the X-ray geometry used to define the system. For these reasons, we conclude that agreement between experiment and theory for the <sup>207</sup>Pb principal components of a chemical-shift tensor of ±5% is agreement within the current levels of combined uncertainty.

## 5. Conclusions

We have presented predictions of <sup>207</sup>Pb magnetic-shielding (and chemical-shift) tensors using a cluster model for network solids. For such network solids, one must deal appropriately

with termination of the cluster to obtain a reasonable SCF solution to the many-body equation. From the test calculations on various clusters, the predicted principal components are not dependent on the termination scheme when a cluster containing atoms through the fifth co-ordination geometry is employed. For all termination schemes, the agreement between experiment and calculation improves as larger clusters are employed. Most errors due to truncation of the structure are minimized if one uses clusters terminated at the third co-ordination shell or higher. Including only the first co-ordination sphere in a cluster is usually not sufficient to account for longer-range effects.

For the solid systems which evince large variation in bond lengths in the structure, modification of terminal-atom nuclear charge by a bond valence model, VMVA/BV, allows one to obtain meaningful SCF solutions for clusters of network solids. In particular, in this work, principal components of the shielding tensor for various lead-containing solids are computed with reasonable accuracy. Although the current investigation is limited to the shielding tensor, we feel this method may be appropriate for computations of localized properties such as spin-spin couplings or surface reaction energetics.



For the prediction of  $^{207}\text{Pb}$  shielding parameters in various systems, we show that it is possible to obtain reasonably quantitative agreement with experiment by calculations with this method applied to clusters that contain at least the third co-ordination shell, provided the full spin-orbit ZORA Hamiltonian at the BP86 level of theory is used. The correlation between experiment and prediction still does not approach the ideal case, showing that other factors influence the calculation.

We have examined factors that may affect the agreement between prediction and experiment. Aside from the inclusion of spin-orbit effects, the most significant source of disagreement of predicted and experimental values arises from the use of the GGA density functional. Considerable improvement of the correlation between experimental and calculated spans results from employing the B3LYP hybrid functional.

An important consideration in the determination of the reliability of calculational techniques is the precision of experimental determinations of parameters, which is difficult for these very broad powder patterns. In one instance, independent determinations of the principal components of the chemical-shift tensor of the two forms of PbO show that there is a substantial variation of the experimental values to which the predicted values are to be compared. This experimental uncertainty is of the order of the variation of predicted values due to variation of structural parameters upon which the calculation is based.

## Acknowledgements

This work was supported by the National Science Foundation under Grant CHE-0956006. The authors thank Dr Shi Bai and Mr Sean Holmes for helpful discussions about the details of these calculations, Dr Eric van Lenthe for helpful discussions of pseudo-atom properties in calculation with the ADF program, and Ms Ozlem K. Alkan for help in writing programs to evaluate bond strengths of terminal atoms which allow prediction of the modified terminal atom charges.

## References

- P. G. Harrison, *Organometallic Compounds of Germanium, Tin, and Lead*, Chapman and Hall, London, 1985.
- A. F. Wells, *Structural Inorganic Chemistry*, Oxford University Press, Oxford, 5th edn, 1984.
- C. Brevard and P. Granger, *Handbook of High Resolution Multinuclear NMR*, John Wiley & Sons, New York, 1981.
- K. J. D. MacKenzie and M. E. Smith, *Multinuclear Solid-State NMR of Inorganic Materials*, Pergamon, Amsterdam, 2002.
- G. Neue, C. Dybowski, M. L. Smith, M. A. Hepp and D. L. Perry, *Solid State Nucl. Magn. Reson.*, 1996, **6**, 241–250.
- F. Fayon, I. Farnan, C. Bessada, J. Coutures, D. Massiot and J. P. Coutures, *J. Am. Chem. Soc.*, 1997, **119**, 6837–6843.
- C. Dybowski, M. L. Smith, M. A. Hepp, E. J. Gaffney, G. Neue and D. L. Perry, *Appl. Spectrosc.*, 1998, **52**, 426–429.
- S. P. Gabuda, S. G. Kozlova, V. V. Terskikh, C. Dybowski, G. Neue and D. L. Perry, *Chem. Phys. Lett.*, 1999, **305**, 353–358.
- S. P. Gabuda, S. G. Kozlova, V. V. Terskikh, C. Dybowski, G. Neue and D. L. Perry, *Solid State Nucl. Magn. Reson.*, 1999, **15**, 103–107.
- C. Dybowski, S. P. Gabuda, S. G. Kozlova, G. Neue, D. L. Perry and V. V. Terskikh, *J. Solid State Chem.*, 2001, **157**, 220–224.
- C. Dybowski and G. Neue, *Prog. Nucl. Magn. Reson. Spectrosc.*, 2002, **41**, 153–170.
- S. E. Van Brammer, A. Glatfelter, S. Bai, C. Dybowski, G. Neue and D. L. Perry, *Magn. Reson. Chem.*, 2006, **44**, 357–365.
- G. G. Briand, A. D. Smith, G. Schatte, A. J. Rossini and R. W. Schurko, *Inorg. Chem.*, 2007, **46**, 8625–8637.
- O. Dmitrenko, S. Bai, P. A. Beckmann, S. van Brammer, A. J. Vega and C. Dybowski, *J. Phys. Chem. A*, 2008, **112**, 3046–3052.
- B. J. Greer, V. K. Michaelis, M. J. Katz, D. B. Leznoff, G. Schreckenbach and S. Kroecker, *Chem. – Eur. J.*, 2011, **17**, 3609–3618.
- J. Catalano, A. Murphy, Y. Yao, G. P. A. Yap, N. Zumbulyadis, S. A. Centeno and C. Dybowski, *Dalton Trans.*, 2015, **44**, 2340–2347.
- A. Rodriguez-Forteza, P. Alemany and T. Ziegler, *J. Phys. Chem. A*, 1999, **103**, 8288–8294.
- A. M. Orendt and J. C. Facelli, *Annu. Rep. NMR Spectrosc.*, 2007, **62**, 115–178.
- F. Alkan and C. Dybowski, *Phys. Chem. Chem. Phys.*, 2014, **16**, 14298–14308.
- C. J. Pickard and F. Mauri, *Phys. Rev. B: Condens. Matter Mater. Phys.*, 2001, **63**, 13.
- D. Sebastiani and M. Parrinello, *J. Phys. Chem. A*, 2001, **105**, 1951–1958.
- D. Sebastiani, G. Goward, I. Schnell and M. Parrinello, *Comput. Phys. Commun.*, 2002, **147**, 707–710.
- C. Bonhomme, C. Gervais, F. Babonneau, C. Coelho, F. Pourpoint, T. Azais, S. E. Ashbrook, J. M. Griffin, J. R. Yates, F. Mauri and C. J. Pickard, *Chem. Rev.*, 2012, **112**, 5733–5779.
- J. A. Tossell, *J. Magn. Reson.*, 1997, **127**, 49–53.
- G. Valerio, A. Goursot, R. Vetrivel, O. Malkina, V. Malkin and D. R. Salahub, *J. Am. Chem. Soc.*, 1998, **120**, 11426–11431.
- J. A. Tossell, *Chem. Phys. Lett.*, 1999, **303**, 435–440.
- J. A. Tossell, *Phys. Chem. Miner.*, 1999, **27**, 70–80.
- G. Valerio and A. Goursot, *J. Phys. Chem. B*, 1999, **103**, 51–58.
- Y. Zhang and E. Oldfield, *J. Phys. Chem. B*, 2004, **108**, 19533–19540.
- M. Body, G. Silly, C. Legein and J. Y. Buzare, *J. Phys. Chem. B*, 2005, **109**, 10270–10278.
- D. Stueber, *Concepts Magn. Reson., Part A*, 2006, **28**, 347–368.
- O. Dmitrenko, S. Bai and C. Dybowski, *Solid State Nucl. Magn. Reson.*, 2008, **34**, 186–190.
- R. E. Taylor, C. T. Carver, R. E. Larsen, O. Dmitrenko, S. Bai and C. Dybowski, *J. Mol. Struct.*, 2009, **930**, 99–109.
- J. Weber and J. Gunne, *Phys. Chem. Chem. Phys.*, 2010, **12**, 583–603.



- 35 A. J. Rossini, A. W. Macgregor, A. S. Smith, G. Schatte, R. W. Schurko and G. G. Briand, *Dalton Trans.*, 2013, **42**, 9533–9546.
- 36 R. E. Taylor, F. Alkan, D. Koumoulis, M. P. Lake, D. King, C. Dybowski and L. S. Bouchard, *J. Phys. Chem. C*, 2013, **117**, 8959–8967.
- 37 Y. Zhang, S. Mukherjee and E. Oldfield, *J. Am. Chem. Soc.*, 2005, **127**, 2370–2371.
- 38 S. Adiga, D. Aebi and D. L. Bryce, *Can. J. Chem.*, 2007, **85**, 496–505.
- 39 N. F. Ramsey, *Phys. Rev.*, 1950, **78**, 699–703.
- 40 R. Ditchfield, *Mol. Phys.*, 1974, **27**, 789–807.
- 41 K. Wolinski, J. F. Hinton and P. Pulay, *J. Am. Chem. Soc.*, 1990, **112**, 8251–8260.
- 42 V. G. Malkin, O. L. Malkina, M. E. Casida and D. R. Salahub, *J. Am. Chem. Soc.*, 1994, **116**, 5898–5908.
- 43 D. H. Brouwer and G. D. Enright, *J. Am. Chem. Soc.*, 2008, **130**, 3095–3105.
- 44 V. M. Bermudez, *J. Phys. Chem. C*, 2010, **114**, 3063–3074.
- 45 M. Casarin, C. Maccato and A. Vittadini, *Inorg. Chem.*, 2000, **39**, 5232–5237.
- 46 M. Casarin, C. Maccato and A. Vittadini, *J. Phys. Chem. B*, 2002, **106**, 795–802.
- 47 M. Casarin, D. Falcomer, A. Glisenti and A. Vittadini, *Inorg. Chem.*, 2003, **42**, 436–445.
- 48 *ADF2014*, SCM, Theoretical Chemistry, Vrije Universiteit, Amsterdam, The Netherlands, 2014, <http://www.scm.com>.
- 49 C. F. Guerra, J. G. Snijders, G. te Velde and E. J. Baerends, *Theor. Chem. Acc.*, 1998, **99**, 391–403.
- 50 G. te Velde, F. M. Bickelhaupt, E. J. Baerends, C. F. Guerra, S. J. A. Van Gisbergen, J. G. Snijders and T. Ziegler, *J. Comput. Chem.*, 2001, **22**, 931–967.
- 51 G. Schreckenbach and T. Ziegler, *J. Phys. Chem.*, 1995, **99**, 606–611.
- 52 G. Schreckenbach and T. Ziegler, *Int. J. Quantum Chem.*, 1996, **60**, 753–766.
- 53 G. Schreckenbach and T. Ziegler, *Theor. Chem. Acc.*, 1998, **99**, 71–82.
- 54 S. K. Wolff, T. Ziegler, E. van Lenthe and E. J. Baerends, *J. Chem. Phys.*, 1999, **110**, 7689–7698.
- 55 J. Autschbach and E. Zurek, *J. Phys. Chem. A*, 2003, **107**, 4967–4972.
- 56 J. P. Perdew, *Phys. Rev. B: Condens. Matter Mater. Phys.*, 1986, **33**, 8822–8824.
- 57 A. D. Becke, *Phys. Rev. A: At., Mol., Opt. Phys.*, 1988, **38**, 3098–3100.
- 58 E. Van lenthe, E. J. Baerends and J. G. Snijders, *J. Chem. Phys.*, 1993, **99**, 4597–4610.
- 59 E. Vanlenthe, E. J. Baerends and J. G. Snijders, *J. Chem. Phys.*, 1994, **101**, 9783–9792.
- 60 E. van Lenthe, R. van Leeuwen, E. J. Baerends and J. G. Snijders, *Int. J. Quantum Chem.*, 1996, **57**, 281–293.
- 61 E. vanLenthe, J. G. Snijders and E. J. Baerends, *J. Chem. Phys.*, 1996, **105**, 6505–6516.
- 62 J. Leciejewicz, *Acta Crystallogr.*, 1961, **14**, 1304.
- 63 P. Garnier, J. Moreau and J. R. Gavarri, *Mater. Res. Bull.*, 1990, **25**, 979–986.
- 64 J. R. Gavarri and D. Weigel, *J. Solid State Chem.*, 1975, **13**, 252–257.
- 65 J. R. Gavarri, J. P. Vigouroux, G. Calvarin and A. W. Hewat, *J. Solid State Chem.*, 1981, **36**, 81–90.
- 66 Y. Z. Nozik, L. E. Fykin and L. A. Muradyan, *Kristallografiya*, 1976, **21**, 76–79.
- 67 M. Lumbreras, J. Protas, S. Jebbari, G. J. Dirksen and J. Schoonman, *Solid State Ionics*, 1986, **20**, 295–304.
- 68 L. Ehm, K. Knorr, F. Madler, H. Voigtlander, E. Busetto, A. Cassetta, A. Lausi and B. Winkler, *J. Phys. Chem. Solids*, 2003, **64**, 919–925.
- 69 H. D. Lutz, K. Beckenkamp, T. Kellersohn, H. Moller and S. Peter, *J. Solid State Chem.*, 1996, **124**, 155–161.
- 70 M. L. Boucher and D. R. Peacor, *Z. Kristallogr., Kristallgeom., Kristallphys., Kristallchem.*, 1968, **126**, 98–111.
- 71 U. Keppler, *Z. Kristallogr., Kristallgeom., Kristallphys., Kristallchem.*, 1970, **132**, 228–235.
- 72 I. D. Brown and R. D. Shannon, *Acta Crystallogr., Sect. A: Cryst. Phys., Diffr., Theor. Gen. Crystallogr.*, 1973, **29**, 266–282.
- 73 I. D. Brown and K. K. Wu, *Acta Crystallogr., Sect. B: Struct. Crystallogr. Cryst. Chem.*, 1976, **32**, 1957–1959.
- 74 I. D. Brown and D. Altermatt, *Acta Crystallogr., Sect. B: Struct. Crystallogr. Cryst. Chem.*, 1985, **41**, 244–247.
- 75 I. D. Brown, *Chem. Rev.*, 2009, **109**, 6858–6919.
- 76 J. Mason, *Solid State Nucl. Magn. Reson.*, 1993, **2**, 285–288.
- 77 U. Haeberlen, *High Resolution NMR in Solids: Selective Averaging*, Academic Press, New York, 1976.
- 78 J. C. Facelli, *Prog. Nucl. Magn. Reson. Spectrosc.*, 2010, **58**, 176–201.
- 79 P. D. Zhao, S. Prasad, J. Huang, J. J. Fitzgerald and J. S. Shore, *J. Phys. Chem. B*, 1999, **103**, 10617–10626.
- 80 Calculations through the fifth co-ordination shell are carried out in Section 4.3 for several systems. The results demonstrate that calculations through the third co-ordination shell account for most of the magnetic shielding with reasonable computational time.
- 81 J. Autschbach and S. Zheng, *Annu. Rep. NMR Spectrosc.*, 2009, **67**, 1–95.
- 82 V. Arcisauskaitė, J. I. Melo, L. Hemmingsen and S. P. A. Sauer, *J. Chem. Phys.*, 2011, **135**, 11.
- 83 J. Roukala, A. F. Maldonado, J. Vaara, G. A. Aucar and P. Lantto, *Phys. Chem. Chem. Phys.*, 2011, **13**, 21016–21025.
- 84 A. Wodynski, M. Repisky and M. Pecul, *J. Chem. Phys.*, 2012, **137**, 11.
- 85 J. Autschbach, *Philos. Trans. R. Soc., A*, 2014, **372**, 39.
- 86 P. Pykko, *Chem. Phys.*, 1983, **74**, 1–7.
- 87 R. Fukuda, M. Hada and H. Nakatsuji, *J. Chem. Phys.*, 2003, **118**, 1027–1035.
- 88 R. Fukuda, M. Hada and H. Nakatsuji, *J. Chem. Phys.*, 2003, **118**, 1015–1026.
- 89 J. Autschbach, *Principles and Applications of Density Functional Theory in Inorganic Chemistry I*, 2004, vol. 112, pp. 1–48.
- 90 A. Bagno, G. Casella and G. Saielli, *J. Chem. Theory Comput.*, 2006, **2**, 37–46.



- 91 J. Autschbach, *Theor. Chem. Acc.*, 2004, **112**, 52–57.
- 92 S. T. Holmes, R. J. Iuliucci, K. T. Mueller and C. Dybowski, *J. Chem. Phys.*, 2014, **141**, 12.
- 93 B. E. G. Lucier, K. E. Johnston, W. Q. Xu, J. C. Hanson, S. D. Senanayake, S. Y. Yao, M. W. Bourassa, M. Srebro, J. Autschbach and R. W. Schurko, *J. Am. Chem. Soc.*, 2014, **136**, 1333–1351.
- 94 C. T. Lee, W. T. Yang and R. G. Parr, *Phys. Rev. B: Condens. Matter Mater. Phys.*, 1988, **37**, 785–789.
- 95 A. D. Becke, *J. Chem. Phys.*, 1993, **98**, 5648–5652.

